Title

Measurement of $\psi(2S)$ meson production in pp collisions at

Journal

European Physical Journal C, 72(8)

ISSN

1434-6044

Authors

The LHCb Collaboration

Aaij, R

Abellan Beteta, C

et al.

Publication Date

2012-08-01

DOI

10.1140/epjc/s10052-012-2100-4

Peer reviewed

Eur. Phys. J. C (2012) 72:2100
DOI 10.1140/epjc/s10052-012-2100-4

THE EUROPEAN PHYSICAL JOURNAL C

Regular Article - Experimental Physics

Measurement of $\psi(2S)$ meson production in pp collisions at $\sqrt{s} = 7$ TeV

The LHCb Collaboration[*]

CERN, 1211 Geneva 23, Switzerland

Received: 11 April 2012 / Revised: 22 May 2012 / Published online: 10 August 2012

Abstract The differential cross-section for the inclusive production of $\psi(2S)$ mesons in pp collisions at $\sqrt{s} = 7$ TeV has been measured with the LHCb detector. The data sample corresponds to an integrated luminosity of 36 pb^{-1}. The $\psi(2S)$ mesons are reconstructed in the decay channels $\psi(2S) \to \mu^+\mu^-$ and $\psi(2S) \to J/\psi\pi^+\pi^-$, with the J/ψ meson decaying into two muons. Results are presented both for promptly produced $\psi(2S)$ mesons and for those originating from b-hadron decays. In the kinematic range $p_{\mathrm{T}}(\psi(2S)) \leq 16$ GeV/c and $2 < y(\psi(2S)) \leq 4.5$ we measure

$$\sigma_{\mathrm{prompt}}\big(\psi(2S)\big) = 1.44 \pm 0.01\ (\mathrm{stat}) \pm 0.12\ (\mathrm{syst})^{+0.20}_{-0.40}\ (\mathrm{pol})\ \mu\mathrm{b},$$

$$\sigma_b\big(\psi(2S)\big) = 0.25 \pm 0.01\ (\mathrm{stat}) \pm 0.02\ (\mathrm{syst})\ \mu\mathrm{b},$$

where the last uncertainty on the prompt cross-section is due to the unknown $\psi(2S)$ polarization. Recent QCD calculations are found to be in good agreement with our measurements. Combining the present result with the LHCb J/ψ measurements we determine the inclusive branching fraction

$$\mathcal{B}\big(b \to \psi(2S)X\big) = \big(2.73 \pm 0.06\ (\mathrm{stat}) \pm 0.16\ (\mathrm{syst}) \pm 0.24\ (\mathrm{BF})\big) \times 10^{-3},$$

where the last uncertainty is due to the $\mathcal{B}(b \to J/\psi X)$, $\mathcal{B}(J/\psi \to \mu^+\mu^-)$ and $\mathcal{B}(\psi(2S) \to e^+e^-)$ branching fraction uncertainties.

1 Introduction

Since its discovery, heavy quarkonium has been one of the most important test laboratories for the development of QCD at the border between the perturbative and non-perturbative regimes, resulting in the formulation of the non-relativistic QCD (NRQCD) factorisation formalism [1, 2]. However, prompt production studies carried out at the Tevatron collider in the early 1990s [3] made clear that NRQCD calculations, based on the leading-order (LO) colour-singlet model (CSM), failed to describe the absolute value and the transverse momentum (p_{T}) dependence of the charmonium production cross-section and polarization data. Subsequently, the inclusion of colour-octet amplitudes in the NRQCD model has reduced the discrepancy between theory and experiment, albeit at the price of tuning *ad hoc* some matrix elements [2]. On the other hand, recent computations of the next-to-leading-order (NLO) and next-to-next-to-leading-order (NNLO) terms in the CSM yielded predictions in better agreement with experimental data, thus resurrecting interest in the colour-singlet framework. Other models have been proposed and it is important to test them in the LHC energy regime [4, 5].

Heavy quarkonium is also produced from b-hadron decays. It can be distinguished from promptly produced quarkonium exploiting its finite decay time. QCD predictions are based on the Fixed-Order-Next-to-Leading-Log (FONLL) approximation for the $b\bar{b}$ production cross-section. The FONLL approach improves NLO results by resumming p_{T} logarithms up to the next-to-leading order [6, 7].

To allow a comparison with theory, promptly produced quarkonia should be separated from those coming from b-hadron decays and from those cascading from higher mass states (feed-down). The latter contribution strongly affects J/ψ production and complicates the interpretation of prompt J/ψ data. On the other hand, $\psi(2S)$ charmonium has no appreciable feed-down from higher mass states and therefore the results can be directly compared with the theoretical predictions, making it an ideal laboratory for QCD studies.

This paper presents a measurement of the $\psi(2S)$ meson production cross-section in pp collisions at the centre-of-

[*] e-mail: decapua.stefano@gmail.com

mass energy $\sqrt{s} = 7$ TeV. The data were collected by the LHCb experiment in 2010 and correspond to an integrated luminosity of 35.9 ± 1.3 pb^{-1}. The analysis is similar to that described in Ref. [8] for the J/ψ production studies; in particular, the separation between promptly produced $\psi(2S)$ and those originating from b-hadron decays is based on the reconstructed decay vertex information. Two decay modes of the $\psi(2S)$ meson have been used: $\psi(2S) \to \mu^+\mu^-$ and $\psi(2S) \to J/\psi\pi^+\pi^-$ followed by $J/\psi \to \mu^+\mu^-$. The $J/\psi\pi^+\pi^-$ mode, despite a larger background and a lower reconstruction efficiency, is used to cross-check and average the results, and to extend the accessible phase space. The production of $\psi(2S)$ meson at the LHC has also been studied at the CMS experiment [9].

2 The LHCb detector and data sample

The LHCb detector is a forward spectrometer [10], designed for precision studies of *CP* violation and rare decays of b- and c-hadrons. Its tracking acceptance covers approximately the pseudorapidity region $2 < \eta < 5$. The detector elements are placed along the beam line of the LHC starting with the vertex detector, a silicon strip device that surrounds the pp interaction region and is positioned at 8 mm from the beams during collisions. It provides precise measurements of the positions of the primary pp interaction vertices and decay vertices of long-lived hadrons, and contributes to the measurement of particle momenta. Other detectors used for momentum measurement include a large area silicon strip detector located before a dipole magnet of approximately 4 Tm, and a combination of silicon strip detectors and straw drift chambers placed downstream. Two ring imaging Cherenkov detectors are used to identify charged hadrons. Further downstream an electromagnetic calorimeter is used for photon and electron detection, followed by a hadron calorimeter. The muon detection consists of five muon stations equipped with multi-wire proportional chambers, with the exception of the centre of the first station using triple-GEM detectors.

The LHCb trigger system consists of a hardware level, based on information from the calorimeter and the muon systems and designed to reduce the frequency of accepted events to a maximum of 1 MHz, followed by a software level which applies a full event reconstruction. In the first stage of the software trigger a partial event reconstruction is performed. The second stage performs a full event reconstruction to further enhance the signal purity.

The analysis uses events selected by single muon or dimuon triggers. The hardware trigger requires one muon candidate with a p_{T} larger than 1.4 GeV/c or two muon candidates with a p_{T} larger than 560 MeV/c and 480 MeV/c. In the first stage of the software trigger, either of the two following selections is required. The first selection confirms the single muon trigger candidate and applies a harder cut on the muon p_{T} at 1.8 GeV/c. The second selection confirms the dimuon trigger candidate by requiring the opposite charge of the two muons and adds a requirement to the dimuon mass to be greater than 2.5 GeV/c^2. In the second stage of the software trigger, two selections are used for the $\psi(2S) \to \mu^+\mu^-$ mode. The first tightens the requirement on the dimuon mass to be greater than 2.9 GeV/c^2 and it applies to the first 8 pb^{-1} of the data sample. Since this selection was subsequently prescaled by a factor five, for the largest fraction of the remaining data (28 pb^{-1}) a different selection is used, which in addition requires a good quality primary vertex and tracks for the dimuon system. For the $J/\psi\pi^+\pi^-$ mode only one selection is used which requires the combined dimuon mass to be in a ± 120 MeV/c^2 mass window around the nominal J/ψ mass. To avoid that a few events with high occupancy dominate the software trigger CPU time, a set of global event cuts is applied on the hit multiplicity of each subdetector used by the pattern recognition algorithms, effectively rejecting events with a large number of pile-up interactions.

The simulation samples used for this analysis are based on the PYTHIA 6.4 generator [11] configured with the parameters detailed in Ref. [12]. The prompt charmonium production processes activated in PYTHIA are those from the leading-order colour-singlet and colour-octet mechanisms. Their implementation and the parameters used are described in detail in Ref. [13]. The EVTGEN package [14] is used to generate hadron decays and the GEANT4 package [15] for the detector simulation. The QED radiative corrections to the decays are generated using the PHOTOS package [16].

3 Signal yield

The two modes, $\psi(2S) \to \mu^+\mu^-$ and $\psi(2S) \to J/\psi\pi^+\pi^-$, have different decay and background characteristics, therefore dedicated selection criteria have been adopted. The optimisation of the cuts has been performed using the simulation. A common requirement is that the tracks, reconstructed in the full tracking system and passing the trigger requirements, must be of good quality ($\chi^2/\mathrm{ndf} < 4$, where ndf is the number of degrees of freedom) and share the same vertex with fit probability $P(\chi^2) > 0.5$ % ($\psi(2S) \to \mu^+\mu^-$) and $P(\chi^2) > 5$ % ($\psi(2S) \to J/\psi\pi^+\pi^-$). A cut $p_{\mathrm{T}} > 1.2$ GeV/c is applied for the muons from the $\psi(2S) \to \mu^+\mu^-$ decay. For muons from $J/\psi(\mu^+\mu^-)\pi^+\pi^-$ we require a momentum larger than 8 GeV/c and $p_{\mathrm{T}} > 0.7$ GeV/c. Finally the rapidity of the reconstructed $\psi(2S)$ is required to satisfy the requirement $2 < y \leq 4.5$.

The $\psi(2S) \to \mu^+\mu^-$ invariant mass spectrum for all selected candidates is shown in Fig. 1(a). The fitting function

is a Crystal Ball [17] describing the signal plus an exponential function for the background. In total 90600 ± 690 signal candidates are found in the $p_{\rm T}$ range 0–12 GeV/c. The mass resolution is 16.01 ± 0.12 MeV/c^2 and the Crystal Ball parameters that account for the radiative tail are obtained from the simulation.

For the $\psi(2S) \to J/\psi(\mu^+\mu^-)\pi^+\pi^-$ decay, both pions are required to have $p_{\rm T} > 0.3$ GeV/c and the sum of the two-pion transverse momenta is required to be larger than 0.8 GeV/c. The quantity $Q = M(J/\psi\pi^+\pi^-) - M(\pi^+\pi^-) - M(\mu^+\mu^-)$ is required to be $\leq$200 MeV/c^2 and to improve the mass resolution the dimuon invariant mass $M_{\mu^+\mu^-}$ is constrained in the fit to the nominal J/ψ mass value [18]. Finally, both J/ψ and $\psi(2S)$ candidates must have $p_{\rm T} > 2$ GeV/c. The invariant mass spectrum is shown in Fig. 1(b) for all selected candidates. For this decay mode the peak is described by the sum of two Crystal Ball functions for the signal plus an exponential function for the background. The number of signal candidates is 12300 ± 200, the mass resolution is 2.10 ± 0.07 MeV/c^2, and the Crystal Ball tail parameters are fixed to the values obtained from the simulation.

The fits are repeated in each $\psi(2S)$ $p_{\rm T}$ bin to obtain the number of signal and background candidates for both decays.

4 Cross-section measurement

The differential cross-section for the inclusive $\psi(2S)$ meson production is computed from

$$\frac{d\sigma}{dp_{\rm T}}(p_{\rm T}) = \frac{N_{\rm sig}(p_{\rm T})}{\mathcal{L}\epsilon_{\rm tot}(p_{\rm T})\mathcal{B}\Delta p_{\rm T}} \tag{1}$$

where $d\sigma/dp_{\rm T}$ is the average cross-section in the given $p_{\rm T}$ bin, integrated over the rapidity range $2 < y \leq 4.5$, $N_{\rm sig}(p_{\rm T})$ is the number of signal candidates determined from the mass fit for the decay under study, $\epsilon_{\rm tot}(p_{\rm T})$ is the total detection efficiency including acceptance and trigger effects, $\mathcal{B}$ denotes the relevant branching fraction and $\Delta p_{\rm T}$ is the bin size. All branching fractions are taken from Ref. [18]: $\mathcal{B}(\psi(2S) \to e^+e^-) = (7.72 \pm 0.17) \times 10^{-3}$, $\mathcal{B}(\psi(2S) \to J/\psi\pi^+\pi^-) = (33.6 \pm 0.4) \times 10^{-2}$ and $\mathcal{B}(J/\psi \to \mu^+\mu^-) = (5.93 \pm 0.06) \times 10^{-2}$. Assuming lepton universality, we use the dielectron branching fraction $\mathcal{B}(\psi(2S) \to e^+e^-)$ in Eq. (1), since $\mathcal{B}(\psi(2S) \to \mu^+\mu^-)$ is less precisely known. $\mathcal{L}$ is the integrated luminosity, which is calibrated using both Van der Meer scans [19, 20] and a beam-profile method [21]. A detailed description of the two methods is given in Ref. [22]. The knowledge of the absolute luminosity scale is used to calibrate the number of tracks in the vertex detector, which is found to be stable throughout the data taking period and can therefore be used to monitor the instantaneous luminosity of the entire data sample. The integrated luminosity of the data sample used in this analysis is determined to be 35.9 pb^{-1}.

The total efficiency, $\epsilon_{\rm tot}(p_{\rm T})$, is a product of three contributions: the geometrical acceptance, the combined detection, reconstruction and selection efficiency, and the trigger efficiency. Each contribution has been determined using simulated events for the two decay channels. In order to evaluate the trigger efficiency, the trigger selection algorithms used during data taking are applied to the simulation.

The total efficiency vs. $p_{\rm T}$ for the two channels, assuming the $\psi(2S)$ meson unpolarized, is shown in Fig. 2. Extensive studies on dimuon decays of prompt J/ψ [8], $\psi(2S)$ and Υ [23] mesons have shown that the total efficiency in the LHCb detector depends strongly on the initial polarization state of the vector meson. This effect is absent for $\psi(2S)$ mesons coming from b-hadron decays. In fact for these events the natural polarization axis is the $\psi(2S)$ meson flight direction in the b-hadron rest frame, while the $\psi(2S)$ meson appears unpolarized along its flight direction in the laboratory. Simulations [8] and measurements from CDF [24] confirm this. We do not measure the $\psi(2S)$ meson polarization but we assign a systematic uncertainty to the unpolarized efficiencies in the case of prompt production. Events are generated with polarizations corresponding to the two extreme cases of fully transverse or fully longitudinal polarization and the efficiency is re-evaluated. The difference between these results and those with the unpolarized sample is taken as an estimate of the systematic uncertainty.

A similar effect exists for the J/ψ meson emitted in the $\psi(2S) \to J/\psi(\mu^+\mu^-)\pi^+\pi^-$ decay. However, in this case, the $\psi(2S)$ meson polarization is fully transferred to the J/ψ meson since, as measured by the BES collaboration [25], the two pions are predominantly in the S-wave configuration[1] and the dipion-J/ψ system is also in a S-wave configuration. This has been verified with data and is correctly reproduced by the simulation. Therefore the systematics due to polarization are fully correlated between the two channels and we use the systematic uncertainties computed for $\psi(2S) \to \mu^+\mu^-$ also for the $\psi(2S) \to J/\psi\pi^+\pi^-$ decay.

In order to separate prompt $\psi(2S)$ mesons from those produced in b-hadron decays, we use the pseudo-decay-time variable defined as $t = d_z(M/p_z)$, where d_z is the separation along the beam axis between the $\psi(2S)$ decay vertex and the primary vertex, M is the nominal mass of the $\psi(2S)$ and p_z is the component of its momentum along the beam axis. In case of multiple primary vertices reconstructed in the same event, that which minimises $|d_z|$ has been chosen. The prompt component is distributed as a Gaussian function around $t = 0$, with width corresponding to the experi-

[1] The small fraction of D-wave measured in Ref. [25] has a negligible impact on our conclusion.

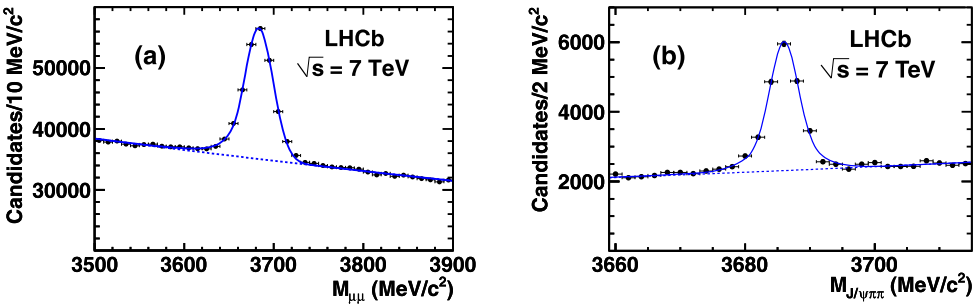

Fig. 1 Invariant mass distribution for all $\psi(2S)$ candidates passing the selection cuts for the $\mu^+\mu^-$ decay (**a**) and the $J/\psi(\mu^+\mu^-)\pi^+\pi^-$ decay (**b**)

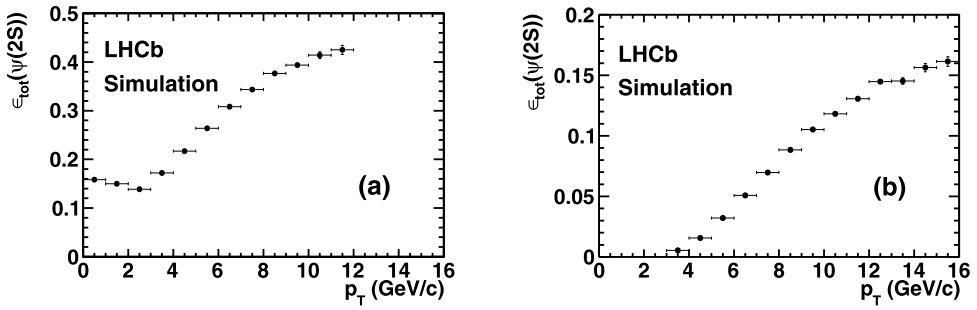

Fig. 2 Total efficiency vs. p_{T} computed from simulation for unpolarized $\psi(2S)$ mesons for $\psi(2S) \to \mu^+\mu^-$ (**a**) and $\psi(2S) \to J/\psi(\mu^+\mu^-)\pi^+\pi^-$ (**b**)

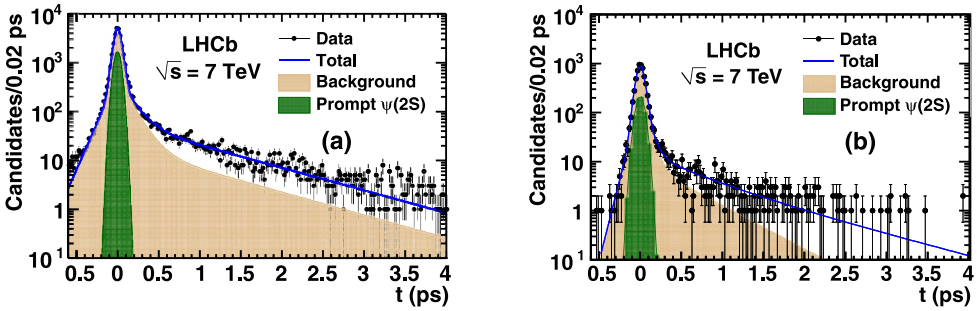

Fig. 3 Pseudo-decay-time distribution for $\psi(2S) \to \mu^+\mu^-$ (**a**) and $\psi(2S) \to J/\psi\pi^+\pi^-$ (**b**) in the p_{T} range $4 < p_{\mathrm{T}} \leq 5$ GeV/c, showing the background and prompt contributions

mental resolution, while for the $\psi(2S)$ from b-hadron decays the t variable is distributed according to an approximately exponential decay law, smeared in the fit with the experimental resolution. The choice of taking the primary vertex which minimises $|d_z|$ could in principle introduce a background component in the pseudo-decay-time distribution arising from the association of the $\psi(2S)$ vertex to a wrong primary vertex. The effect of such background is found to be of the order of 0.5 % in the region around $t = 0$ and has been neglected. The function used to fit the t distribution in each p_{T} bin is

$$
\begin{aligned}
&F(t;\, f_{\mathrm{p}}, \sigma, \tau_b) \\
&= N_{\mathrm{sig}}\left[f_{\mathrm{p}}\delta(t) + (1 - f_{\mathrm{p}})\theta(t)\frac{e^{-\frac{t}{\tau_b}}}{\tau_b} \right] \otimes \frac{e^{-\frac{1}{2}(\frac{t}{\sigma})^2}}{\sqrt{2\pi}\sigma} \\
&\quad + N_{\mathrm{bkg}} f_{\mathrm{bkg}}(t; \boldsymbol{\Theta})
\end{aligned}
\tag{2}
$$

where N_{sig} and N_{bkg} are respectively the numbers of signal and background candidates obtained from the mass fit. The fit parameters are the prompt fraction, f_{p}, the standard deviation of the Gaussian resolution function, σ, and the lifetime describing the long-lived component of $\psi(2S)$ mesons coming from b-hadron decays, τ_b. In principle, all fit parameters are dependent on p_{T}. The function $f_{\mathrm{bkg}}(t; \boldsymbol{\Theta})$ models the background component in the distribution and is defined as the sum of a δ function and a Gaussian function for the prompt background, plus two exponential functions for the positive tail and one exponential function for the negative tail, all convolved with a Gaussian function to account for the detector resolution. The array of parameters $\boldsymbol{\Theta}$ is determined from a fit to the t distribution of the events in the mass sidebands.

As an example, the pseudo-decay-time distributions for $\psi(2S) \to \mu^+\mu^-$ and $\psi(2S) \to J/\psi\pi^+\pi^-$ in the p_{T} range $4 < p_{\mathrm{T}} \leq 5$ GeV/c are presented in Fig. 3. The contributions of background and prompt $\psi(2S)$ mesons are also shown. The values of the prompt fraction, f_{p} vs. p_{T} in the rapidity range $2 < y \leq 4.5$, obtained for the $\mu^+\mu^-$ and the $J/\psi\pi^+\pi^-$ modes, are in good agreement as shown in Fig. 4.

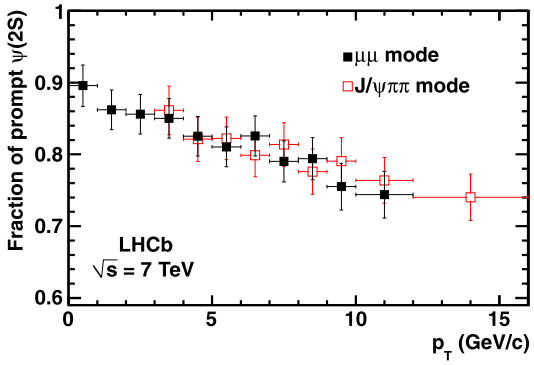

Fig. 4 Fraction of prompt $\psi(2S)$ as a function of p_{T} for the $\mu^+\mu^-$ mode (*solid squares*) and the $J/\psi\pi^+\pi^-$ mode (*open squares*). *Error bars* include the statistical uncertainties and the systematic uncertainties due to the fitting procedure

5 Systematic uncertainties on the cross-section measurement

A variety of sources of systematic uncertainties affecting the cross-section measurement were taken into account and are summarised in Table 1.

A thorough analysis of the luminosity scans yields consistent results for the absolute luminosity scale with a precision of 3.5 % [22], this value being assigned as a systematic uncertainty. The statistical uncertainties from the finite number of simulated events on the efficiencies are included as a source of systematic uncertainty; this uncertainty varies from 0.4 to 2.2 % for the $\mu^+\mu^-$ mode and from 0.6 to 1 % for the $J/\psi\pi^+\pi^-$ mode. In addition, we assign a systematic uncertainty in order to account for the difference between the trigger efficiency evaluated on data by means of an unbiased $\mu^+\mu^-$ sample, and the trigger efficiency computed from the simulation. This results in a bin-dependent uncertainty up to 8 % for the $\mu^+\mu^-$ mode and up to 7 % for the $J/\psi\pi^+\pi^-$ mode. This uncertainty is fully correlated between the two decay modes in the overlapping p_{T} region. Finally, the statistical uncertainty on the global event cuts efficiency (2.1 % for both modes) is taken as an additional systematic uncertainty [8].

To assess possible systematic differences in the acceptance between data and simulation for the $J/\psi\pi^+\pi^-$ mode, we have studied the dipion mass distribution. The LHCb simulation is based on the Voloshin-Zakharov model [26] which uses a single phenomenological parameter λ

$$\frac{d\sigma}{dm_{\pi\pi}} \propto \Phi(m_{\pi\pi})\left[m_{\pi\pi}^2 - \lambda m_{\pi}^2\right]^2, \tag{3}$$

where $\Phi(m_{\pi\pi})$ is a phase space factor (see e.g. Ref. [25]) and in the simulation $\lambda = 4$ is assumed. The dipion mass distribution obtained from the data is shown in Fig. 5. We obtain $\lambda = 4.46 \pm 0.07$ (stat) ± 0.18 (syst), from which we estimate a negligible systematic effect on the acceptance (0.25%). Our result is also in good agreement with the BES value $\lambda = 4.36 \pm 0.06$ (stat) ± 0.17(syst) [25].

Table 1 Systematic uncertainties included in the measurement of the cross-section. Uncertainties labelled with *a* are correlated between the $\mu^+\mu^-$ and $J/\psi\pi^+\pi^-$ mode, while *b* indicates a correlation between $\psi(2S) \to \mu^+\mu^-$ and the $J/\psi \to \mu^+\mu^-$ uncertainties [8]

Uncertainty source	$\mu^+\mu^-$ (%)	$J/\psi\pi^+\pi^-$ (%)
Luminosity[a,b]	3.5	3.5
Size of simulation sample	0.4–2.2	0.6–1.0
Trigger efficiency[a]	1–8	1–7
Global event cuts[a,b]	2.1	2.1
Muon identification[a,b]	1.1	1.1
Hadron identification	–	0.5
Track χ^2[a,b]	1	2
Tracking efficiency[a]	3.5	7.3
Vertex fit[b]	0.8	1.3
Unknown polarization[a]	15–26	15–26
Mass fit function	1.1	0.5
Pseudo-decay-time fits	2.7	2.7
$\mathcal{B}(\psi(2S) \to e^+e^-)$	2.2	–
$\mathcal{B}(\psi(2S) \to J/\psi\pi^+\pi^-)$	–	1.2
$\mathcal{B}(J/\psi \to \mu^+\mu^-)$	–	1.0

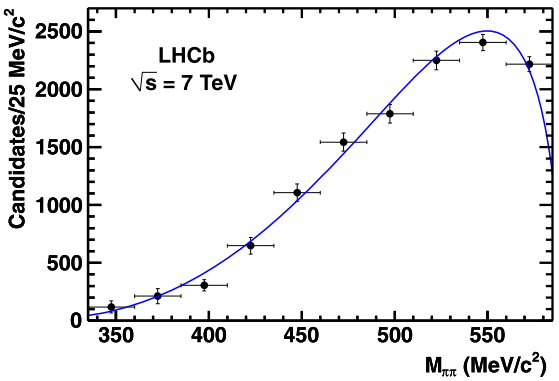

Fig. 5 Dipion mass spectrum for the $\psi(2S) \to J/\psi\pi^+\pi^-$ decay. The *curve* shows the result of the fit with Eq. (3) corrected for the acceptance

To cross-check and assign a systematic uncertainty to the determination of the muon identification efficiency from simulation, the single track muon identification efficiency has been measured on data using a tag-and-probe method [27]. This gives a correction factor for the dimuon of 1.025 ± 0.011, which we apply to the simulation efficiencies. The 1.1 % uncertainty on the correction factor is used as systematic uncertainty. The efficiency of the selection requirement on the dipion identification has been studied on data and simulation and a difference of 1 % has been measured between the two. Therefore, the simulation effi-

ciencies are corrected for this difference and an additional systematic uncertainty of 0.5 % is included.

The $\psi(2S)$ selection also includes a requirement on the track fit quality. The relative difference between the efficiency of this requirement in simulation and data is taken as a systematic uncertainty, resulting in an uncertainty of 0.5 % per track. Tracking studies show that the ratio of the track-finding efficiencies between data and simulation is 1.09 for the $\mu^+\mu^-$ mode and 1.06 for the $J/\psi\pi^+\pi^-$ mode, with an uncertainty of 3.5 % and 7.3 % respectively; the simulation efficiencies are corrected accordingly and the corresponding systematic uncertainties are included.

For the requirement on the secondary vertex fit quality, a relative difference of 1.6 % for the $\mu^+\mu^-$ mode and 2.6 % for the $J/\psi\pi^+\pi^-$ mode has been measured between data and simulation. The simulation efficiency is therefore corrected for this difference and a corresponding systematic uncertainty of 0.8 % ($\mu^+\mu^-$) and 1.3 % ($J/\psi\pi^+\pi^-$) is assigned.

The systematic uncertainty due to the unknown polarization is computed as discussed in Sect. 4. The study done for the two extreme polarization hypotheses gives an average systematic uncertainty between 15 % and 26 % for both modes, relative to the hypothesis of zero polarization, depending on the p_{T} bin. These errors are fully correlated between the two decay modes and strongly asymmetric since the variations of the efficiency are of different magnitude for transverse and longitudinal polarizations.

A systematic uncertainty from the fitting procedure has been estimated from the relative difference between the overall number of signal $\psi(2S)$ and the number of signal candidates obtained by summing the results of the fits in the individual p_{T} bins. A total systematic uncertainty of 1.1 % for the $\mu^+\mu^-$ mode and 0.5 % for the $J/\psi\pi^+\pi^-$ mode is assigned.

Finally, to evaluate the systematic uncertainty on the prompt fraction from the $\psi(2S)$ pseudo-decay-time fit we recompute f_{p} with τ_b (see Eq. (2)) fixed to the largest and smallest value obtained in the p_{T}-bin fits. The relative variation is at most 2.7 % and this value is assigned as a systematic uncertainty on f_{p}.

6 Cross-section results

The differential cross-sections for prompt $\psi(2S)$ and $\psi(2S)$ mesons from b-hadron decays are shown in Fig. 6, where we compare the results obtained for the $\psi(2S) \to \mu^+\mu^-$ and $\psi(2S) \to J/\psi\pi^+\pi^-$ channels separately for the prompt and b-hadron decay components.

The values for the two cross-sections estimated using the different decay modes are consistent within 0.5 σ. A weighted average of the two measurements is performed to extract the final result listed in Table 2.

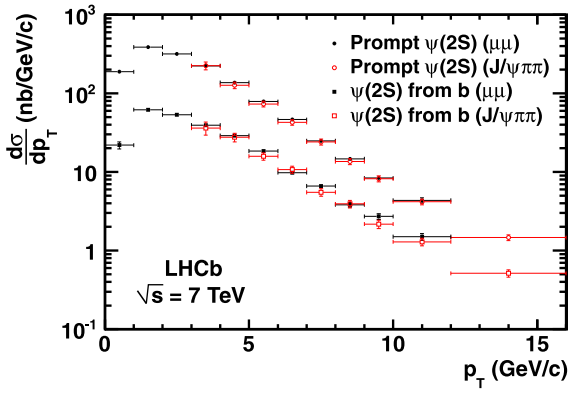

Fig. 6 Comparison of the differential cross-sections measured for prompt $\psi(2S)$ (*circles*) and for $\psi(2S)$ from b-hadron decay (*squares*) in the $\psi(2S) \to \mu^+\mu^-$ (*solid symbols*) and $\psi(2S) \to J/\psi\pi^+\pi^-$ (*open symbols*) modes. Only the uncorrelated uncertainties are shown

Table 2 Cross-section values for prompt $\psi(2S)$ and $\psi(2S)$ from b-hadrons in different p_{T} bins and in the range $2 < y \leq 4.5$, evaluated as the weighted average of the $\mu^+\mu^-$ and $J/\psi\pi^+\pi^-$ channels. The first error is statistical, the second error is systematic, and the last asymmetric uncertainty is due to the unknown polarization of the prompt $\psi(2S)$ meson

p_{T} [GeV/c]	$\frac{d\sigma_{\mathrm{prompt}}}{dp_{\mathrm{T}}}$ [$\frac{\mathrm{nb}}{\mathrm{GeV}/c}$]	$\frac{d\sigma_{\mathrm{b}}}{dp_{\mathrm{T}}}$ [$\frac{\mathrm{nb}}{\mathrm{GeV}/c}$]
0–1	$188 \pm 6 \pm 18^{+32}_{-67}$	$22 \pm 2 \pm 2$
1–2	$387 \pm 8 \pm 37^{+60}_{-119}$	$62 \pm 3 \pm 6$
2–3	$317 \pm 7 \pm 26^{+44}_{-88}$	$53 \pm 2 \pm 4$
3–4	$224 \pm 6 \pm 24^{+27}_{-53}$	$39 \pm 2 \pm 4$
4–5	$135 \pm 4 \pm 13^{+16}_{-30}$	$29 \pm 1 \pm 3$
5–6	$77 \pm 2 \pm 7^{+9}_{-18}$	$18 \pm 1 \pm 2$
6–7	$46 \pm 1 \pm 4^{+5}_{-10}$	$10 \pm 1 \pm 1$
7–8	$25 \pm 1 \pm 2^{+3}_{-6}$	$6.3 \pm 0.4 \pm 0.5$
8–9	$14 \pm 1 \pm 1^{+2}_{-3}$	$3.9 \pm 0.3 \pm 0.3$
9–10	$8.3 \pm 0.4 \pm 0.7^{+0.9}_{-1.7}$	$2.5 \pm 0.2 \pm 0.2$
10–12	$4.3 \pm 0.3 \pm 0.4^{+0.5}_{-0.9}$	$1.4 \pm 0.1 \pm 0.1$
12–16	$1.5 \pm 0.1 \pm 0.2^{+0.2}_{-0.3}$	$0.51 \pm 0.04 \pm 0.06$

The differential cross-section for promptly produced $\psi(2S)$ mesons, along with a comparison with some recent theory predictions [28–31] tuned to the LHCb acceptance, is shown in Fig. 7. In Refs. [28] and [29] the differential prompt cross-section has been computed up to NLO terms in nonrelativistic QCD, including colour-singlet and colour-octet contributions. In Refs. [30, 31] the prompt cross-section has been evaluated in a colour-singlet framework, including up to the dominant α_s^5 NNLO terms. Experimentally the large-p_{T} tail behaves like $p_{\mathrm{T}}^{-\beta}$ with $\beta = 4.2 \pm 0.6$ and is rather well reproduced, especially in the colour-octet models.

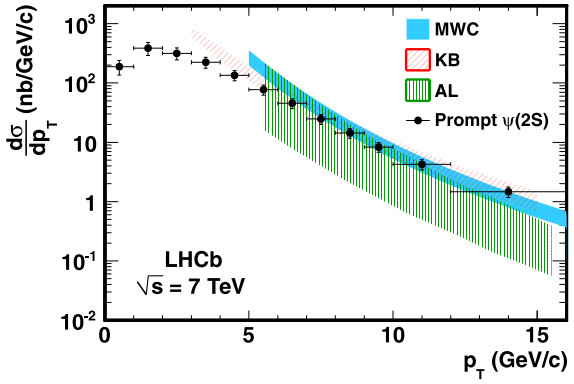

Fig. 7 Differential production cross-section vs. p_{T} for prompt $\psi(2S)$. The predictions of three nonrelativistic QCD models are also shown for comparison. MWC [28] and KB [29] are NLO calculations including colour-singlet and colour-octet contributions. AL [30, 31] is a colour-singlet model including the dominant NNLO terms

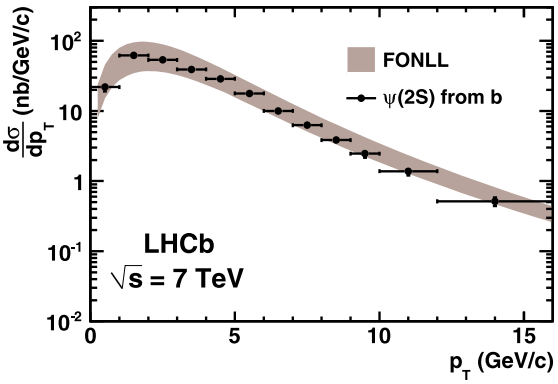

Fig. 8 Differential production cross-section vs. p_{T} for $\psi(2S)$ from b-hadrons. The shaded band is the prediction of a FONLL calculation [6, 7, 32]

The differential cross-section for $\psi(2S)$ produced in b-hadron decays and the comparison with a recent theory prediction [32] based on the FONLL approach [6, 7] are presented in Fig. 8. The theoretical prediction of Ref. [32] uses as input the $b \to \psi(2S)X$ branching fraction obtained in the following section. Experimentally the $\psi(2S)$ mesons resulting from b-hadron decay have a slightly harder p_{T} spectrum than those produced promptly: $\beta = 3.6 \pm 0.5$. By integrating the differential cross-section for prompt $\psi(2S)$ and $\psi(2S)$ from b-hadrons in the range $2 < y \leq 4.5$ and $p_{\mathrm{T}} \leq 16\ \mathrm{GeV}/c$, we obtain

$$\sigma_{\mathrm{prompt}}\big(\psi(2S)\big) = 1.44 \pm 0.01\ (\mathrm{stat}) \pm 0.12\ (\mathrm{syst})^{+0.20}_{-0.40}\ (\mathrm{pol})\ \mu\mathrm{b},$$

$$\sigma_b\big(\psi(2S)\big) = 0.25 \pm 0.01\ (\mathrm{stat}) \pm 0.02\ (\mathrm{syst})\ \mu\mathrm{b},$$

where the systematic uncertainty includes all the sources listed in Table 1, except for the polarization, while the last asymmetric uncertainty is due to the effect of the unknown $\psi(2S)$ polarization and applies only to the prompt component.

7 Inclusive $b \to \psi(2S)X$ branching fraction measurement

The inclusive branching fraction for a b-hadron decaying to $\psi(2S)$ is presently known with 50 % precision: $\mathcal{B}(b \to \psi(2S)X) = (4.8 \pm 2.4) \times 10^{-3}$ [18]. Combining the present result for $\sigma_b(\psi(2S))$ with the previous measurement of $\sigma_b(J/\psi)$ [8] we can obtain an improved value of the aforementioned branching fraction. To achieve this, it is necessary to extrapolate the two measurements to the full phase space. The extrapolation factors for the two decays have been determined using the LHCb simulation [12] and they have been found to be $\alpha_{4\pi}(J/\psi) = 5.88$ [8] and $\alpha_{4\pi}(\psi(2S)) = 5.48$. Most of the theoretical uncertainties are expected to cancel in the ratio of the two factors $\xi = \alpha_{4\pi}(\psi(2S))/\alpha_{4\pi}(J/\psi) = 0.932$, which is used in Eq. (4). A systematic uncertainty of 3.4 % is estimated for this correction and included in the final result below. Therefore

$$\frac{\mathcal{B}(b \to \psi(2S)X)}{\mathcal{B}(b \to J/\psi X)} = \xi \frac{\sigma_b(\psi(2S))}{\sigma_b(J/\psi)}. \tag{4}$$

For $\sigma_b(J/\psi)$ we rescale the value in [8] for the new determination of the integrated luminosity ($\mathcal{L} = 5.49 \pm 0.19\ \mathrm{pb}^{-1}$). For $\sigma_b(\psi(2S))$ we use only the data from the $\psi(2S) \to \mu^+\mu^-$ mode to cancel most of the systematic uncertainties in the ratio. Effects due to polarization are negligible for mesons resulting from b-hadron decay. We obtain

$$\frac{\mathcal{B}(b \to \psi(2S)X)}{\mathcal{B}(b \to J/\psi X)} = 0.235 \pm 0.005\ (\mathrm{stat}) \pm 0.015\ (\mathrm{syst}),$$

where the correlated uncertainties (Table 1) between the two cross-sections are excluded. By inserting the value $\mathcal{B}(b \to J/\psi X) = (1.16 \pm 0.10) \times 10^{-2}$ [18] we get

$$\mathcal{B}\big(b \to \psi(2S)X\big) = \big(2.73 \pm 0.06\ (\mathrm{stat}) \pm 0.16\ (\mathrm{syst}) \pm 0.24\ (\mathrm{BF})\big) \times 10^{-3},$$

where the last uncertainty originates from the uncertainty of the branching fractions $\mathcal{B}(b \to J/\psi X)$, $\mathcal{B}(\psi(2S) \to e^+e^-)$ and $\mathcal{B}(J/\psi \to \mu^+\mu^-)$.

The ratio of the $\psi(2S) \to \mu^+\mu^-$ to $J/\psi \to \mu^+\mu^-$ differential cross-sections is shown vs. p_{T} in Fig. 9 for prompt production (R_{p}, Fig. 9(a)) and when the vector mesons originate from b-hadron decays (R_b, Fig. 9(b)). Since it is not known if the promptly produced $\psi(2S)$ and J/ψ have similar polarizations [33], we do not assume any correlation of the polarization uncertainties when computing the uncertainties on R_{p}. The increase of $R_{\mathrm{p}(b)}$ with p_{T} is similar to that measured in the central rapidity region by the CDF [24] and CMS [9] collaborations.

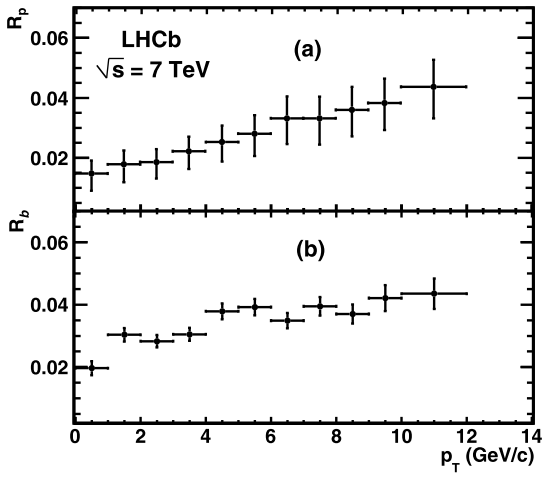

Fig. 9 Ratio of $\psi(2S) \to \mu^+\mu^-$ to $J/\psi \to \mu^+\mu^-$ cross-sections for prompt production (**a**) and for b-hadron decay (**b**), as a function of p_{T}

8 Conclusions

We have measured the differential cross-section for the process $pp \to \psi(2S)X$ at the centre-of-mass energy of 7 TeV, as a function of the transverse momentum in the range $p_{\mathrm{T}}(\psi(2S)) \leq 16$ GeV/c and $2 < y(\psi(2S)) \leq 4.5$, via the decay modes $\psi(2S) \to \mu^+\mu^-$ and $\psi(2S) \to J/\psi\pi^+\pi^-$. The data sample corresponds to about 36 pb^{-1} collected by the LHCb experiment at the LHC. Results from the two decay modes agree. The $\psi(2S)$ prompt cross-section has been separated from the cross-section of $\psi(2S)$ from b-hadrons through the study of the pseudo-decay-time and the two measurements have been averaged. In the above kinematic range we measure

$$\sigma_{\mathrm{prompt}}\big(\psi(2S)\big) = 1.44 \pm 0.01\ (\mathrm{stat}) \pm 0.12\ (\mathrm{syst})^{+0.20}_{-0.40}\ (\mathrm{pol})\ \mu\mathrm{b},$$

$$\sigma_b\big(\psi(2S)\big) = 0.25 \pm 0.01\ (\mathrm{stat}) \pm 0.02\ (\mathrm{syst})\ \mu\mathrm{b}.$$

The measured $\psi(2S)$ production cross-sections are in good agreement with the results of several recent NRQCD calculations. In addition, we obtain an improved value for the $b \to \psi(2S)X$ branching fraction by combining the two LHCb production cross-section measurements of the two vector mesons J/ψ and $\psi(2S)$ from b-hadrons. The result,

$$\mathcal{B}\big(b \to \psi(2S)X\big) = \big(2.73 \pm 0.06\ (\mathrm{stat}) \pm 0.16\ (\mathrm{syst}) \pm 0.24\ (\mathrm{BF})\big) \times 10^{-3},$$

is in good agreement with recent results from the CMS collaboration [9] and is a significant improvement over the present PDG average [18].

Acknowledgements We express our gratitude to our colleagues in the CERN accelerator departments for the excellent performance of the LHC. We thank the technical and administrative staff at CERN and at the LHCb institutes, and acknowledge support from the National Agencies: CAPES, CNPq, FAPERJ and FINEP (Brazil); CERN; NSFC (China); CNRS/IN2P3 (France); BMBF, DFG, HGF and MPG (Germany); SFI (Ireland); INFN (Italy); FOM and NWO (The Netherlands); SCSR (Poland); ANCS (Romania); MinES of Russia and Rosatom (Russia); MICINN, XUNGAL and GENCAT (Spain); SNSF and SER (Switzerland); NAS Ukraine (Ukraine); STFC (United Kingdom); NSF (USA). We also acknowledge the support received from the ERC under FP7 and the Region Auvergne.

We thank B. Kniehl, M. Butenschön and M. Cacciari for providing theoretical predictions of $\psi(2S)$ cross-sections in the LHCb acceptance range.

References

1. W.E. Caswell, G.P. Lepage, Effective lagrangians for bound state problems in QED, QCD, and other field theories. Phys. Lett. B **167**, 437 (1986)
2. G.T. Bodwin, E. Braaten, G.P. Lepage, Rigorous QCD analysis of inclusive annihilation and production of heavy quarkonium. Phys. Rev. D **51**, 1125 (1995) [Erratum: Phys. Rev. D **55**, 5853 (1997)]. arXiv:hep-ph/9407339
3. F. Abe et al. (CDF Collaboration), Inclusive J/ψ, $\psi(2S)$, and b-quark production in $\bar{p}p$ collisions at $\sqrt{s} = 1.8$ TeV. Phys. Rev. Lett. **69**, 3704 (1992)
4. N. Brambilla et al., Heavy quarkonium physics (2005). arXiv:hep-ph/0412158v2
5. N. Brambilla et al., Heavy quarkonium: progress, puzzles and opportunities (2010). arXiv:1010.5827v1 [hep-ph]
6. M. Cacciari, M. Greco, P. Nason, The p_{T} spectrum in heavy-flavour hadroproduction. J. High Energy Phys. **9805**, 007 (1998)
7. M. Cacciari, S. Frixione, M. Mangano, P. Nason, G. Ridolfi, QCD analysis of first b cross section data at 1.96 TeV. J. High Energy Phys. **0407**, 033 (2004)
8. R. Aaij et al. (LHCb Collaboration), Measurement of J/ψ production in pp collisions at $\sqrt{s} = 7$ TeV. Eur. Phys. J. C **71**, 1645 (2011)
9. S. Chatrchyan et al. (CMS Collaboration), J/ψ and $\psi(2S)$ production in pp collisions at $\sqrt{s} = 7$ TeV. J. High Energy Phys. **02**, 11 (2011)
10. A.A. Alves Jr. et al. (LHCb Collaboration), The LHCb detector at the LHC. J. Instrum. **3**, S08005 (2008)
11. I. Belyaev et al., Handling of the generation of primary events in GAUSS, the LHCb simulation framework, in *Nuclear Science Symposium Conference Record (NSS/MIC)* (IEEE, New York, 2010), p. 1155
12. M. Clemencic et al., The LHCb simulation application, gauss: design, evolution and experience. J. Phys. Conf. Ser. **331**, 3032023 (2011)
13. M. Bargiotti, V. Vagnoni, Heavy quarkonia sector in PYTHIA 6.324: tuning, validation and perspectives at LHCb. CERN-LHCb-2007-042
14. D.J. Lange, The EvtGen particle decay simulation package. Nucl. Instrum. Methods A **462**, 152 (2001)
15. S. Agostinelli et al. (GEANT4 Collaboration), GEANT4: a simulation toolkit. Nucl. Instrum. Methods A **506**, 250 (2003)
16. P. Golonka, Z. Was, PHOTOS Monte Carlo: a precision tool for QED corrections in Z and W decays. Eur. Phys. J. C **45**, 97 (2006)

17. T. Skwarnicki, A study of the radiative cascade transitions between the Upsilon-prime and upsilon resonances. PhD thesis, Institute of Nuclear Physics, Krakow, 1986. DESY-F31-86-02
18. K. Nakamura et al. (Particle Data Group), Review of particle physics. J. Phys. G **37**, 075201 (2010)
19. S. Van der Meer, Calibration of the effective beam height in the ISR. CERN report, ISR-PO/68-31 (1968)
20. H. Burkhardt, P. Grafström, Absolute luminosity from machine parameters. CERN-LHC-PROJECT-Report-1019 (2007)
21. M. Ferro-Luzzi, Proposal for an absolute luminosity determination in colliding beam experiments using vertex detection of beam-gas interactions. Nucl. Instrum. Methods A **553**, 388–399 (2005)
22. R. Aaij et al. (LHCb Collaboration), Absolute luminosity measurements with the LHCb detector at the LHC. J. Instrum. **7**, P01010 (2012)
23. R. Aaij et al. (LHCb Collaboration), Measurement of Υ. production in pp collisions at $\sqrt{s} = 7$ TeV. arXiv:1202.6579v1 [hep-ex]
24. T. Aaltonen et al. (CDF Collaboration), Production of $\psi(2S)$ mesons in $p\bar{p}$ collisions at 1.96 TeV. Phys. Rev. D **80**, 031103 (2009)
25. J. Bai et al. (BES Collaboration), $\pi^+\pi^- J/\psi$ decay distributions. Phys. Rev. D **62**, 032002 (2000)
26. M. Voloshin, V. Zakharov, Measuring quantum-chromodynamic anomalies in hadronic transitions between quarkonium states. Phys. Rev. Lett. **45**, 688–691 (1980)
27. A. Sarti et al., Calibration strategy and efficiency measurement of the muon identification procedure at LHCb. LHCb-PUB-2010-002
28. Y.-Q. Ma, K. Wang, K.-T. Chao, A complete NLO calculation of the J/ψ and ψ' production at hadron colliders. arXiv:1012.1030 [hep-ph]
29. B. Kniehl, M. Butenschön, Reconciling J/ψ production at HERA, RHIC, Tevatron, and LHC with nonrelativistic QCD factorization at next-to-leading order. Phys. Rev. Lett. **106**, 022003 (2011), and private communication
30. P. Artoisenet et al., Υ production at Fermilab Tevatron and LHC energies. Phys. Rev. Lett. **101**, 152001 (2008)
31. J.-P. Lansberg, On the mechanisms of heavy-quarkonium hadroproduction. Eur. Phys. J. C **61**, 693 (2009)
32. M. Cacciari, Private communication
33. A. Abulencia et al. (CDF Collaboration), Polarizations of J/ψ and $\psi(2S)$ mesons produced in $p\bar{p}$ collisions at $\sqrt{s} = 1.96$ TeV. Phys. Rev. Lett. **99**, 132001 (2007)

The LHCb Collaboration

R. Aaij[38], C. Abellan Beteta[33,n], B. Adeva[34], M. Adinolfi[43], C. Adrover[6], A. Affolder[49], Z. Ajaltouni[5], J. Albrecht[35], F. Alessio[35], M. Alexander[48], G. Alkhazov[27], P. Alvarez Cartelle[34], A.A. Alves Jr[22], S. Amato[2], Y. Amhis[36], J. Anderson[37], R.B. Appleby[51], O. Aquines Gutierrez[10], F. Archilli[18,35], L. Arrabito[55,p], A. Artamonov[32], M. Artuso[53,35], E. Aslanides[6], G. Auriemma[22,m], S. Bachmann[11], J.J. Back[45], D.S. Bailey[51], V. Balagura[28,35], W. Baldini[16], R.J. Barlow[51], C. Barschel[35], S. Barsuk[7], W. Barter[44], A. Bates[48], C. Bauer[10], Th. Bauer[38], A. Bay[36], I. Bediaga[1], S. Belogurov[28], K. Belous[32], I. Belyaev[28], E. Ben-Haim[8], M. Benayoun[8], G. Bencivenni[18], S. Benson[47], J. Benton[43], R. Bernet[37], M.-O. Bettler[17], M. van Beuzekom[38], A. Bien[11], S. Bifani[12], T. Bird[51], A. Bizzeti[17,h], P.M. Bjørnstad[51], T. Blake[35], F. Blanc[36], C. Blanks[50], J. Blouw[11], S. Blusk[53], A. Bobrov[31], V. Bocci[22], A. Bondar[31], N. Bondar[27], W. Bonivento[15], S. Borghi[48,51], A. Borgia[53], T.J.V. Bowcock[49], C. Bozzi[16], T. Brambach[9], J. van den Brand[39], J. Bressieux[36], D. Brett[51], M. Britsch[10], T. Britton[53], N.H. Brook[43], H. Brown[49], K. de Bruyn[38], A. Büchler-Germann[37], I. Burducea[26], A. Bursche[37], J. Buytaert[35], S. Cadeddu[15], O. Callot[7], M. Calvi[20,j], M. Calvo Gomez[33,n], A. Camboni[33], P. Campana[18,35], A. Carbone[14], G. Carboni[21,k], R. Cardinale[19,35,i], A. Cardini[15], L. Carson[50], K. Carvalho Akiba[2], G. Casse[49], M. Cattaneo[35], Ch. Cauet[9], M. Charles[52], Ph. Charpentier[35], N. Chiapolini[37], K. Ciba[35], X. Cid Vidal[34], G. Ciezarek[50], P.E.L. Clarke[47,35], M. Clemencic[35], H.V. Cliff[44], J. Closier[35], C. Coca[26], V. Coco[38], J. Cogan[6], P. Collins[35], A. Comerma-Montells[33], F. Constantin[26], A. Contu[52], A. Cook[43], M. Coombes[43], G. Corti[35], B. Couturier[35], G.A. Cowan[36], R. Currie[47], C. D'Ambrosio[35], P. David[8], P.N.Y. David[38], I. De Bonis[4], S. De Capua[21,k], M. De Cian[37], F. De Lorenzi[12], J.M. De Miranda[1], L. De Paula[2], P. De Simone[18], D. Decamp[4], M. Deckenhoff[9], H. Degaudenzi[36,35], L. Del Buono[8], C. Deplano[15], D. Derkach[14,35], O. Deschamps[5], F. Dettori[39], J. Dickens[44], H. Dijkstra[35], P. Diniz Batista[1], F. Domingo Bonal[33,n], S. Donleavy[49], F. Dordei[11], A. Dosil Suárez[34], D. Dossett[45], A. Dovbnya[40], F. Dupertuis[36], R. Dzhelyadin[32], A. Dziurda[23], S. Easo[46], U. Egede[50], V. Egorychev[28], S. Eidelman[31], D. van Eijk[38], F. Eisele[11], S. Eisenhardt[47], R. Ekelhof[9], L. Eklund[48], Ch. Elsasser[37], D. Elsby[42], D. Esperante Pereira[34], A. Falabella[16,14,e], E. Fanchini[20,j], C. Färber[11], G. Fardell[47], C. Farinelli[38], S. Farry[12], V. Fave[36], V. Fernandez Albor[34], M. Ferro-Luzzi[35], S. Filippov[30], C. Fitzpatrick[47], M. Fontana[10], F. Fontanelli[19,i], R. Forty[35], O. Francisco[2], M. Frank[35], C. Frei[35], M. Frosini[17,f], S. Furcas[20], A. Gallas Torreira[34], D. Galli[14,c], M. Gandelman[2], P. Gandini[52], Y. Gao[3], J-C. Garnier[35], J. Garofoli[53], J. Garra Tico[44], L. Garrido[33], D. Gascon[33], C. Gaspar[35], R. Gauld[52], N. Gauvin[36], M. Gersabeck[35], T. Gershon[45,35], Ph. Ghez[4], V. Gibson[44], V.V. Gligorov[35], C. Göbel[54,q], D. Golubkov[28], A. Golutvin[50,28,35], A. Gomes[2], H. Gordon[52], M. Grabalosa Gándara[33], R. Graciani Diaz[33], L.A. Granado Cardoso[35], E. Graugés[33], G. Graziani[17], A. Grecu[26], E. Greening[52], S. Gregson[44], B. Gui[53], E. Gushchin[30], Yu. Guz[32], T. Gys[35], C. Hadjivasiliou[53], G. Haefeli[36], C. Haen[35], S.C. Haines[44], T. Hampson[43], S. Hansmann-Menzemer[11], R. Harji[50], N. Harnew[52], J. Harrison[51], P.F. Harrison[45], T. Hartmann[56,r], J. He[7], V. Heijne[38], K. Hennessy[49], P. Henrard[5], J.A. Hernando Morata[34], E. van Herwijnen[35],

E. Hicks[49], K. Holubyev[11], P. Hopchev[4], W. Hulsbergen[38], P. Hunt[52], T. Huse[49], R.S. Huston[12], D. Hutchcroft[49], D. Hynds[48], V. Iakovenko[41], P. Ilten[12], J. Imong[43], R. Jacobsson[35], A. Jaeger[11], M. Jahjah Hussein[5], E. Jans[38], F. Jansen[38], P. Jaton[36], B. Jean-Marie[7], F. Jing[3], M. John[52], D. Johnson[52], C.R. Jones[44], B. Jost[35], M. Kaballo[9], S. Kandybei[40], M. Karacson[35], T.M. Karbach[9], J. Keaveney[12], I.R. Kenyon[42], U. Kerzel[35], T. Ketel[39], A. Keune[36], B. Khanji[6], Y.M. Kim[47], M. Knecht[36], R.F. Koopman[39], P. Koppenburg[38], M. Korolev[29], A. Kozlinskiy[38], L. Kravchuk[30], K. Kreplin[11], M. Kreps[45], G. Krocker[11], P. Krokovny[11], F. Kruse[9], K. Kruzelecki[35], M. Kucharczyk[20,23,35,j], T. Kvaratskheliya[28,35], V.N. La Thi[36], D. Lacarrere[35], G. Lafferty[51], A. Lai[15], D. Lambert[47], R.W. Lambert[39], E. Lanciotti[35], G. Lanfranchi[18], C. Langenbruch[11], T. Latham[45], C. Lazzeroni[42], R. Le Gac[6], J. van Leerdam[38], J.-P. Lees[4], R. Lefèvre[5], A. Leflat[29,35], J. Lefrançois[7], O. Leroy[6], T. Lesiak[23], L. Li[3], L. Li Gioi[5], M. Lieng[9], M. Liles[49], R. Lindner[35], C. Linn[11], B. Liu[3], G. Liu[35], J. von Loeben[20], J.H. Lopes[2], E. Lopez Asamar[33], N. Lopez-March[36], H. Lu[3], J. Luisier[36], A. Mac Raighne[48], F. Machefert[7], I.V. Machikhiliyan[4,28], F. Maciuc[10], O. Maev[27,35], J. Magnin[1], S. Malde[52], R.M.D. Mamunur[35], G. Manca[15,d], G. Mancinelli[6], N. Mangiafave[44], U. Marconi[14], R. Märki[36], J. Marks[11], G. Martellotti[22], A. Martens[8], L. Martin[52], A. Martín Sánchez[7], D. Martinez Santos[35], A. Massafferri[1], Z. Mathe[12], C. Matteuzzi[20], M. Matveev[27], E. Maurice[6], B. Maynard[53], A. Mazurov[16,30,35], G. McGregor[51], R. McNulty[12], M. Meissner[11], M. Merk[38], J. Merkel[9], R. Messi[21,k], S. Miglioranzi[35], D.A. Milanes[13], M.-N. Minard[4], J. Molina Rodriguez[54,q], S. Monteil[5], D. Moran[12], P. Morawski[23], R. Mountain[53], I. Mous[38], F. Muheim[47], K. Müller[37], R. Muresan[26], B. Muryn[24], B. Muster[36], M. Musy[33], J. Mylroie-Smith[49], P. Naik[43], T. Nakada[36], R. Nandakumar[46], I. Nasteva[1], M. Nedos[9], M. Needham[47], N. Neufeld[35], A.D. Nguyen[36], C. Nguyen-Mau[36,o], M. Nicol[7], V. Niess[5], N. Nikitin[29], A. Nomerotski[52,35], A. Novoselov[32], A. Oblakowska-Mucha[24], V. Obraztsov[32], S. Oggero[38], S. Ogilvy[48], O. Okhrimenko[41], R. Oldeman[15,35,d], M. Orlandea[26], J.M. Otalora Goicochea[2], P. Owen[50], K. Pal[53], J. Palacios[37], A. Palano[13,b], M. Palutan[18], J. Panman[35], A. Papanestis[46], M. Pappagallo[48], C. Parkes[51], C.J. Parkinson[50], G. Passaleva[17], G.D. Patel[49], M. Patel[50], S.K. Paterson[50], G.N. Patrick[46], C. Patrignani[19,i], C. Pavel-Nicorescu[26], A. Pazos Alvarez[34], A. Pellegrino[38], G. Penso[22,l], M. Pepe Altarelli[35], S. Perazzini[14,c], D.L. Perego[20,j], E. Perez Trigo[34], A. Pérez-Calero Yzquierdo[33], P. Perret[5], M. Perrin-Terrin[6], G. Pessina[20], A. Petrella[16,35], A. Petrolini[19,i], A. Phan[53], E. Picatoste Olloqui[33], B. Pie Valls[33], B. Pietrzyk[4], T. Pilař[45], D. Pinci[22], R. Plackett[48], S. Playfer[47], M. Plo Casasus[34], G. Polok[23], A. Poluektov[45,31], E. Polycarpo[2], D. Popov[10], B. Popovici[26], C. Potterat[33], A. Powell[52], J. Prisciandaro[36], V. Pugatch[41], A. Puig Navarro[33], W. Qian[53], J.H. Rademacker[43], B. Rakotomiaramanana[36], M.S. Rangel[2], I. Raniuk[40], G. Raven[39], S. Redford[52], M.M. Reid[45], A.C. dos Reis[1], S. Ricciardi[46], A. Richards[50], K. Rinnert[49], D.A. Roa Romero[5], P. Robbe[7], E. Rodrigues[48,51], F. Rodrigues[2], P. Rodriguez Perez[34], G.J. Rogers[44], S. Roiser[35], V. Romanovsky[32], M. Rosello[33,n], J. Rouvinet[36], T. Ruf[35], H. Ruiz[33], G. Sabatino[21,k], J.J. Saborido Silva[34], N. Sagidova[27], P. Sail[48], B. Saitta[15,d], C. Salzmann[37], M. Sannino[19,i], R. Santacesaria[22], C. Santamarina Rios[34], R. Santinelli[35], E. Santovetti[21,k], M. Sapunov[6], A. Sarti[18,l], C. Satriano[22,m], A. Satta[21], M. Savrie[16,e], D. Savrina[28], P. Schaack[50], M. Schiller[39], S. Schleich[9], M. Schlupp[9], M. Schmelling[10], B. Schmidt[35], O. Schneider[36], A. Schopper[35], M.-H. Schune[7], R. Schwemmer[35], B. Sciascia[18], A. Sciubba[18,l], M. Seco[34], A. Semennikov[28], K. Senderowska[24], I. Sepp[50], N. Serra[37], J. Serrano[6], P. Seyfert[11], M. Shapkin[32], I. Shapoval[40,35], P. Shatalov[28], Y. Shcheglov[27], T. Shears[49], L. Shekhtman[31], O. Shevchenko[40], V. Shevchenko[28], A. Shires[50], R. Silva Coutinho[45], T. Skwarnicki[53], N.A. Smith[49], E. Smith[52,46], K. Sobczak[5], F.J.P. Soler[48], A. Solomin[43], F. Soomro[18,35], B. Souza De Paula[2], B. Spaan[9], A. Sparkes[47], P. Spradlin[48], F. Stagni[35], S. Stahl[11], O. Steinkamp[37], S. Stoica[26], S. Stone[53,35], B. Storaci[38], M. Straticiuc[26], U. Straumann[37], V.K. Subbiah[35], S. Swientek[9], M. Szczekowski[25], P. Szczypka[36], T. Szumlak[24], S. T'Jampens[4], E. Teodorescu[26], F. Teubert[35], C. Thomas[52], E. Thomas[35], J. van Tilburg[11], V. Tisserand[4], M. Tobin[37], S. Topp-Joergensen[52], N. Torr[52], E. Tournefier[4,50], S. Tourneur[36], M.T. Tran[36], A. Tsaregorodtsev[6], N. Tuning[38], M. Ubeda Garcia[35], A. Ukleja[25], P. Urquijo[53], U. Uwer[11], V. Vagnoni[14], G. Valenti[14], R. Vazquez Gomez[33], P. Vazquez Regueiro[34], S. Vecchi[16], J.J. Velthuis[43], M. Veltri[17,g], B. Viaud[7], I. Videau[7], D. Vieira[2], X. Vilasis-Cardona[33,n], J. Visniakov[34], A. Vollhardt[37], D. Volyanskyy[10], D. Voong[43], A. Vorobyev[27], H. Voss[10], S. Wandernoth[11], J. Wang[53], D.R. Ward[44], N.K. Watson[42], A.D. Webber[51], D. Websdale[50], M. Whitehead[45], D. Wiedner[11], L. Wiggers[38], G. Wilkinson[52], M.P. Williams[45,46], M. Williams[50], F.F. Wilson[46], J. Wishahi[9], M. Witek[23], W. Witzeling[35], S.A. Wotton[44], K. Wyllie[35], Y. Xie[47], F. Xing[52], Z. Xing[53], Z. Yang[3], R. Young[47], O. Yushchenko[32], M. Zangoli[14], M. Zavertyaev[10,a], F. Zhang[3], L. Zhang[53], W.C. Zhang[12], Y. Zhang[3], A. Zhelezov[11], L. Zhong[3], A. Zvyagin[35]

[1]Centro Brasileiro de Pesquisas Físicas (CBPF), Rio de Janeiro, Brazil
[2]Universidade Federal do Rio de Janeiro (UFRJ), Rio de Janeiro, Brazil
[3]Center for High Energy Physics, Tsinghua University, Beijing, China
[4]LAPP, Université de Savoie, CNRS/IN2P3, Annecy-Le-Vieux, France
[5]Clermont Université, Université Blaise Pascal, CNRS/IN2P3, LPC, Clermont-Ferrand, France
[6]CPPM, Aix-Marseille Université, CNRS/IN2P3, Marseille, France
[7]LAL, Université Paris-Sud, CNRS/IN2P3, Orsay, France

[8]LPNHE, Université Pierre et Marie Curie, Université Paris Diderot, CNRS/IN2P3, Paris, France
[9]Fakultät Physik, Technische Universität Dortmund, Dortmund, Germany
[10]Max-Planck-Institut für Kernphysik (MPIK), Heidelberg, Germany
[11]Physikalisches Institut, Ruprecht-Karls-Universität Heidelberg, Heidelberg, Germany
[12]School of Physics, University College Dublin, Dublin, Ireland
[13]Sezione INFN di Bari, Bari, Italy
[14]Sezione INFN di Bologna, Bologna, Italy
[15]Sezione INFN di Cagliari, Cagliari, Italy
[16]Sezione INFN di Ferrara, Ferrara, Italy
[17]Sezione INFN di Firenze, Firenze, Italy
[18]Laboratori Nazionali dell'INFN di Frascati, Frascati, Italy
[19]Sezione INFN di Genova, Genova, Italy
[20]Sezione INFN di Milano Bicocca, Milano, Italy
[21]Sezione INFN di Roma Tor Vergata, Roma, Italy
[22]Sezione INFN di Roma La Sapienza, Roma, Italy
[23]Henryk Niewodniczanski Institute of Nuclear Physics Polish Academy of Sciences, Kraków, Poland
[24]AGH University of Science and Technology, Kraków, Poland
[25]Soltan Institute for Nuclear Studies, Warsaw, Poland
[26]Horia Hulubei National Institute of Physics and Nuclear Engineering, Bucharest-Magurele, Romania
[27]Petersburg Nuclear Physics Institute (PNPI), Gatchina, Russia
[28]Institute of Theoretical and Experimental Physics (ITEP), Moscow, Russia
[29]Institute of Nuclear Physics, Moscow State University (SINP MSU), Moscow, Russia
[30]Institute for Nuclear Research of the Russian Academy of Sciences (INR RAN), Moscow, Russia
[31]Budker Institute of Nuclear Physics (SB RAS) and Novosibirsk State University, Novosibirsk, Russia
[32]Institute for High Energy Physics (IHEP), Protvino, Russia
[33]Universitat de Barcelona, Barcelona, Spain
[34]Universidad de Santiago de Compostela, Santiago de Compostela, Spain
[35]European Organization for Nuclear Research (CERN), Geneva, Switzerland
[36]Ecole Polytechnique Fédérale de Lausanne (EPFL), Lausanne, Switzerland
[37]Physik-Institut, Universität Zürich, Zürich, Switzerland
[38]Nikhef National Institute for Subatomic Physics, Amsterdam, The Netherlands
[39]Nikhef National Institute for Subatomic Physics and Vrije Universiteit, Amsterdam, The Netherlands
[40]NSC Kharkiv Institute of Physics and Technology (NSC KIPT), Kharkiv, Ukraine
[41]Institute for Nuclear Research of the National Academy of Sciences (KINR), Kyiv, Ukraine
[42]University of Birmingham, Birmingham, United Kingdom
[43]H.H. Wills Physics Laboratory, University of Bristol, Bristol, United Kingdom
[44]Cavendish Laboratory, University of Cambridge, Cambridge, United Kingdom
[45]Department of Physics, University of Warwick, Coventry, United Kingdom
[46]STFC Rutherford Appleton Laboratory, Didcot, United Kingdom
[47]School of Physics and Astronomy, University of Edinburgh, Edinburgh, United Kingdom
[48]School of Physics and Astronomy, University of Glasgow, Glasgow, United Kingdom
[49]Oliver Lodge Laboratory, University of Liverpool, Liverpool, United Kingdom
[50]Imperial College London, London, United Kingdom
[51]School of Physics and Astronomy, University of Manchester, Manchester, United Kingdom
[52]Department of Physics, University of Oxford, Oxford, United Kingdom
[53]Syracuse University, Syracuse, NY, United States
[54]Pontifícia Universidade Católica do Rio de Janeiro (PUC-Rio), Rio de Janeiro, Brazil
[55]CC-IN2P3, CNRS/IN2P3, Lyon-Villeurbanne, France
[56]Physikalisches Institut, Universität Rostock, Rostock, Germany
[a]P.N. Lebedev Physical Institute, Russian Academy of Science (LPI RAS), Moscow, Russia
[b]Università di Bari, Bari, Italy
[c]Università di Bologna, Bologna, Italy
[d]Università di Cagliari, Cagliari, Italy

[e]Università di Ferrara, Ferrara, Italy
[f]Università di Firenze, Firenze, Italy
[g]Università di Urbino, Urbino, Italy
[h]Università di Modena e Reggio Emilia, Modena, Italy
[i]Università di Genova, Genova, Italy
[j]Università di Milano Bicocca, Milano, Italy
[k]Università di Roma Tor Vergata, Roma, Italy
[l]Università di Roma La Sapienza, Roma, Italy
[m]Università della Basilicata, Potenza, Italy
[n]LIFAELS, La Salle, Universitat Ramon Llull, Barcelona, Spain
[o]Hanoi University of Science, Hanoi, Viet Nam
[p]Associated member
[q]Associated to Universidade Federal do Rio de Janeiro (UFRJ), Rio de Janeiro, Brazil
[r]Associated to Physikalisches Institut, Ruprecht-Karls-Universität Heidelberg, Heidelberg, Germany